Success stories of CFD Modelling in Understanding the Continuous Casting Process: The Impact of Microscopic Dynamics on Macroscopic Scales

Christine Gruber[1,a)], Hadi Barati[1], Gerhard Holzinger[1], Mirko Javurek[2], Xiaomeng Zhang[1], Sergiu Ilie[3], Susanne Michelic[4], Mahdi Saeedipour[5], Menghuai Wu[6]

[1] *K1-MET GmbH, Stahlstr. 14, 4020 Linz, Austria*
[2]*Institute of Fluid Mechanics and Heat Transfer, Johannes Kepler University, Altenbergerstr. 69, 4040 Linz, Austria*
[3] *voestalpine Stahl GmbH, voestalpine-Straße 3, A-4020 Linz, Austria*
[4] *Chair for Ferrous Metallurgy, Montanuniversität Leoben, Franz-Josef-Str. 18, 8700 Leoben, Austria*
[5] *Department of Particulate Flow Modelling, Johannes Kepler University, Altenbergerstr. 69, 4040 Linz, Austria*
[6] *Chair of Modelling and Simulation of Metallurgical Processes, Montanuniversität Leoben, Franz-Josef-Str. 18, 8700 Leoben, Austria*

[a)] Corresponding author: christine.gruber@k1-met.com

Abstract. In this contribution, we will review recent advances and success stories in the CFD modelling of the continuous casting process in the framework of K1-MET projects in Austria. Physical phenomena on both microscopic and macroscopic scales have been investigated, and the resulting dynamics in the metallurgical process sequence of continuous casting has been modelled. Non-metallic inclusions (NMIs), their microscopic dynamics and their interaction with macroscopic flows in casting vessels have strong impact on the final steel quality. If NMIs are not properly treated in the tundish of a continuous caster, e.g., captured by or dissolved in the covering slag, these particles can cause clogging in the submerged entry nozzle (SEN) and lead to harmful defects in the cast steel slab. Therefore, several efforts to model the NMI behaviour using CFD tools to depict their behaviour in a multiphase fluid flow will be reviewed and put into context to each other. These models include NMI removal from the steel into the slag phase in a tundish, their subsequent advance into the SEN and impact on clogging, as well as their behaviour in the mold during the casting and solidification. The different modelling approaches and their respective validation by experiments have been successfully brought together to achieve a comprehensive image of the dynamics governing the complete continuous casting process and are an impressive showcase of the insights into complex industrial processes that can be gained with CFD modelling.

INTRODUCTION

In this paper, we will review CFD-based modelling approaches used for different process stages in continuous casting, taking into account the relevant physics between liquids (steel melt, slag phase), gases (argon injection) and solids (inclusions, refractory vessel walls or other plant components) in each process stage.

Non-metallic inclusions (NMIs) are particles in the form of oxides present in the steel melt and are the reason for undesired effects in the processing of liquid steel, like clogging, and in the final product, like material defects and deficiencies. Sources of NMIs are materials additions in steel processing and refining, interactions of steel and refractory materials and deoxidation and reoxidation processes in the steel melt through contact with air and other gases. NMIs can be removed from liquid steel through the separation at interfaces in the system, like on the surface of gas bubbles or on the interface between two different fluid phases, with the goal of eventually dissolving in the slag phase. This removal via fluid-fluid or fluid-gas interfaces is one of the main purposes of the tundish in continuous casting, besides regulating the flow towards the SEN. If they cannot be removed from the melt in the tundish, detrimental effects on the process and the properties of the final steel product are to be expected.

Clogging, i.e., the deposition of particles at vessel walls, is a particular issue in the SEN, where the attachment of solid particles to the wall eventually hinders the fluid flow into the mold, leading to unstable process conditions. The main mechanism for clogging is likely the transport and deposit of NMIs onto the SEN wall, but also thermochemical reactions between the refractory and the melt at the SEN wall, the oxidation of steel caused by airflow permeating through the porous material of the SEN wall, the precipitation of particles onto the SEN walls due to shifts in chemical conditions at lower temperatures or even the solidification or freezing of melt material onto the SEN walls are relevant

phenomena. Modelling the clogging process under different conditions is thus important to gain insights into the different mechanisms, and to be able to avoid adverse process conditions.

The final possibility to remove NMIs from the steel is in the mold, where they can be transported up towards the meniscus and be absorbed into the mold slag. NMIs which can neither be removed in the tundish, nor deposited in the SEN clog, nor captured by the mold slag, will end up in the cast slab, diminishing the material quality. Inclusions can lead to defects during solidification in the mold and will become visible/ relevant in the later stages of the rolling processes, causing stability failures, cracks, and defects in the final steel product.

Understanding these processes and phenomena in the continuous casting of steel thus requires in-depth modelling on the behavior of multiphase fluid flows, as well as specific knowledge on the materials involved. For the validation of the multiphase fluid models, the analyses of data from the industrial process can yield insights, but also analog models in lab- or plant scale are built, e.g., water-air systems, where the observation of specific phenomena is easier than in a steel-argon system, or also liquid metal setups with low-melting alloys. Knowledge on material properties is obtained from post-mortem laboratory experiments of the melt, refractory materials, and plant components.

In this paper, we will present modelling approaches to depict the behavior of NMIs in multiphase flow systems featuring fluid-fluid and fluid-gas interfaces, clogging, deposition as well as the solidification stage. Models developed on a microscopic scale have been implemented into macroscale setups to evaluate their impact on these scales. Examples of this include the separation of NMIs into gas and slag phase in a generic tundish geometry, the growth of clogging in SENs, as well as the impact of a clogged SEN on the mold flows. In several research activities in the frame of K1-MET projects in Austria, detailed simulations of the NMI behaviour have been developed, characterizing their tendencies of dissolving into a slag phase at the steel-slag interface or adhering to the vessel walls. On the one hand, these success stories will be reviewed here, and on the other hand context and synergies between them will be presented as new contributions. Considering the wettability and size of the particles, as well as local capillary motion and Marangoni convection, an effective removal rate of NMIs from steel into a slag phase has been derived by Zhang et al. These simulations have been validated with laboratory experiments determining separation dynamics as well as material properties, for different combinations of NMI and slag materials. Subsequently, transport of NMIs in the SEN, nozzle clogging considering the transient clog growth and its interaction with the multiphase flow have been modelled by Barati et al. Laboratory investigations of clogged SENs with different material compositions have been compared to the simulations for a validation of the CFD model. Based on these detailed simulations, effective models for the NMI behaviour in tundish and SEN have been developed, and effective NMI removal rates and clogging rates, respectively, have been incorporated into larger-scale simulations to simulate a realistic flow behaviour in vessels like tundish and SEN (work to be published). Mold flow simulations will be reviewed based on the work of Javurek et al. Ultimately, the SEN clogging model has been used as a boundary condition for the effective flow behaviour of steel into the mold, and new results on the impact on the solidification and potential casting defects in the steel slab will be shown.

NUMERICAL MODELLING

Models have been developed for the process stages along the continuous casting process, from NMI separation in the tundish by Zhang et al., to SEN flows and clogging phenomena by Barati et al. and bubbly mold flows by Javurek et al. In this section, we will introduce these detailed models, describe their setup and validity, and comment on their validation with experimental data.

Modelling the NMI separation in multiphase fluid flows

Inclusion removal is an essential function of the tundish stage of continuous casting. Endogenous inclusions like products of chemical reactions (e.g., Al_2O_3) or exogenous inclusion caused by slag entrapment or refractory erosion impact the steel cleanliness and can cause defects and cracks during the solidification or further processing of the steel product. NMI separation in the tundish happens on interfaces in the multiphase flow, like at the steel-slag interface, where they can be absorbed into the tundish slag. In the literature, inclusion removal has been modelled within tundish CFD simulations by the tracking of particle trajectories, removing the particles from the steel when reaching the steel-slag interface [1] [2]. This does not consider effects that happen at the interface: dissolution kinetics, the absorption dynamics or the possibility of particles returning into the steel phase. Furthermore, in another study on the behavior of inclusion particles crossing the metal-slag surface and the forces acting on them [3], the importance of the wettability of particles has been emphasized, but no interface deformation has been assumed, and thus the interfacial forces and particle dynamics have not been fully depicted. Therefore, in several new studies by Zhang et al. these

effects have been considered in numerical investigations of the detailed particle motion at the steel-slag interface [4], leading towards the definition of a small-scale criterion for particle separation for different material properties [5].

The detailed model for inclusion particles at the interface is implemented in a small computational domain using the volume of fluid (VOF) method [6] for an incompressible two-phase flow, with a transport equation for the volume fraction indicating the phase of the fluid. Surface tension has been modelled with the continuum surface force (CSF) model [7], where the wetting angle is introduced as the relevant parameter. In this way, the capillary forces and dynamics created by different wetting angles of the particle in the surrounding fluid can be modelled numerically. Dynamic overset grids have been used to model the particle movement, to achieve a good mesh in the vicinity of the particle surface and allow for a large particle displacement while maintaining mesh quality to account for surface tension effects more accurately.

For simplification, first studies have been done with water-air systems, backed up by analytical considerations. Generalizations towards steel-slag-argon systems have been done subsequently, where the much higher interfacial tension and fluid viscosities lead to different dynamics and dominating effects. CFD studies of steel-slag-argon systems have been backed up by experimental investigations of several exemplary materials relevant in steel continuous casting.

For the numerical method, a pressure-based coupled solver is used along with first-order schemes in temporal and momentum spatial discretization to ensure the stability of the solution. For more accurate VOF solutions, the volume fraction discretization uses the geometric reconstruction scheme, which presents a sharp interface between fluids by a piecewise-linear approach and is the most accurate option available. The least squares cell-based method is chosen for the gradients calculating. Besides, the PRESTO! scheme is used for pressure interpolation, and the least squares method is employed for the overset interface interpolation. Due to the micron-sized mesh grids, very small time steps in the order of 10^{-8} s are applied. The simulations have been carried out using commercial software ANSYS Fluent based on 32 computational cores.

The CFD investigations show the characteristics of the particle dynamics and particle motion across the steel-slag surface, including the behavior of the surrounding meniscus and the influence of the wetting angle, as depicted in several snapshots in Fig.1(a). The process is a very fast motion driven by capillary forces on timescales of the order of milliseconds. Validation of the CFD studies has been done by comparison with analytical consideration of the Young-Laplace equation for water-air systems [5], and good agreement for the obtained capillary forces and meniscus interface deformations has been obtained. In general, the particle dynamics closely correlates with interface deformation, and better slag wettability ("slagophilic" particles) shows favorable separation behavior [4].

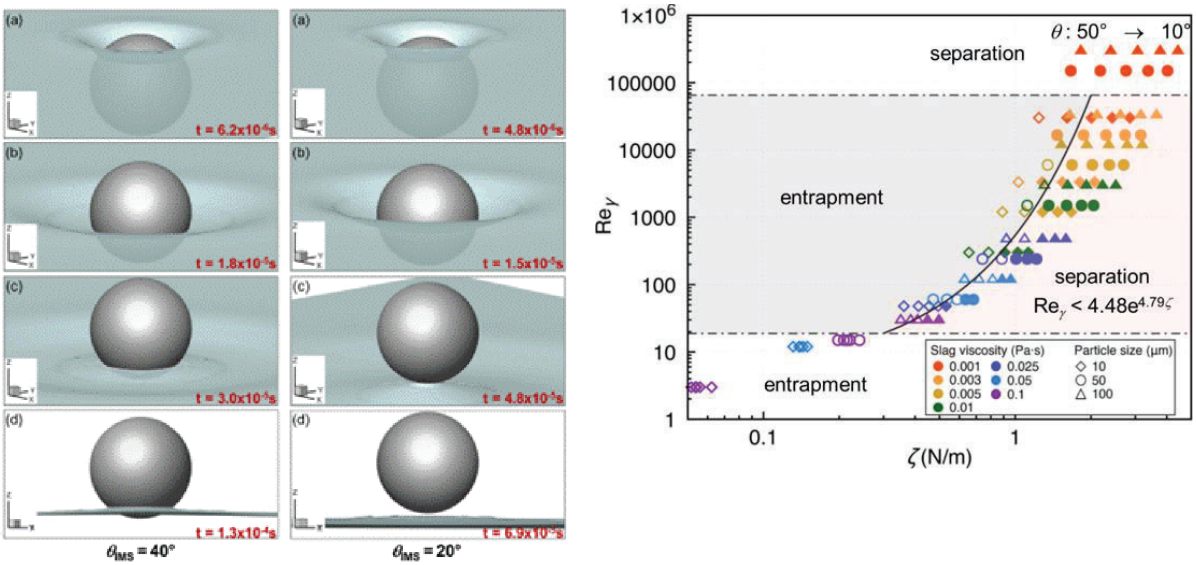

(a) (b)

FIGURE 1. Inclusion removal at steel-slag interface [4]. (a) VOF-overset grid simulation of inclusion particle behavior at the steel-slag interface with different slag wettability: trapped at the interface (left) and separated toward slag (right). (b) Graph of the simulated cases [5] in terms of particle dynamics (ζ) over the surface tension and viscosity effects (Re_γ).

Further investigations have been done towards the definition of a separation criterion for particles on the interface. Extensive parameter studies for different slag viscosities, interfacial tensions and contact angles, as well as particle properties (size, density) have been carried out. The properties of the steel phase have been assumed to be constant, and a series of simulation cases have been done to establish the inclusion dynamics of separation or entrapment at the steel-slag interface. In contrast to systems with small viscosity (e.g., water-air), where capillary forces dominate and hydrophobic particles are easily separated on the interface, in highly viscous systems like in the case of steel and tundish slag, the separation is dominated by both capillary forces and viscosity effects, and entrapment of the particle at the interface can take place. The relative effect of surface tension to viscous force can be described by the ratio of Reynolds number to capillary number,

$$Re_\gamma = \frac{Re}{Ca} = \frac{\rho_S \gamma_{MS} D_I}{\mu_S^2}\,, \tag{1}$$

a dimensionless number, where ρ_S is the density of slag, γ_{MS} is the interfacial tension between metal and slag, D_I is the inclusion size and μ_S is the viscosity of slag. A quantity representing the particle dynamics can be defined as

$$\zeta = \rho_I u_{max}^2 D_I\,, \tag{2}$$

where ρ_I is the density of inclusions, and u_{max} is the maximum particle velocity when crossing the interface. ζ is the kinetic energy of the inclusions divided by the inclusion surface area, i.e., a surface energy (achieving some independence of the inclusion size) and has turned out as a useful criterion to visually separate different inclusion behavior in dependence on material properties in a plot of Re_γ over ζ, where either separation or entrapment will take place depending on the combination of material parameters. Figure 1(b) shows the relation of Re_γ and ζ. For the regions on the top and on the right, separation of inclusions into the slag phase takes place, whereas for the other regions, inclusions tend to be trapped at the interface. Different wetting angles θ (five data points in each horizontal line for angles varying from 50° to 10°) and inclusion sizes (different symbol shapes) have been considered. The most relevant parameter is slag viscosity (denoted by different colors), and it can be shown that for realistic tundish slag viscosities $\mu_S \gtrsim 0.1\ Pa \cdot s$, it is difficult regardless of the wetting angle and inclusion size to achieve a separation of inclusions into the slag. The solid curve in the graph is a data fit distinguishing inclusion separation and entrapment in the respective simulations, with particles separated if their parameters satisfy $Re_\gamma < 4.48\, e^{4.79\,\zeta}$. The two regions at the top and bottom of the graph represent separation or entrapment regardless of ζ.

The key parameters for particle separation are those parameters that lead to maximum displacement, i.e., the contact angle and the slag viscosity. From this criterion, a probability for separation can be extracted, which can then be applied in larger-scale simulations without the need to resolve the micro-scale dynamics of inclusion separation. Specifically, the combination of slag parameters, interfacial tension, inclusion properties, and the separation criterion leads to a dependence of u_{max} on these parameters, which can be used in large scale simulation cases. The outcome will be discussed further in one of the next subsections.

The subsequent stage of dissolution of inclusion particles happening in the slag phase was further considered in [8]. Here, Marangoni convection induced by interfacial tension gradients was investigated. Such gradients around an inclusion particle trigger an interfacial flow towards high interfacial tension regions. This was modelled by the transport equation for the mass fraction of dissolving species and an additional source term for Marangoni force in momentum equation. The particle detachment at the interface involves a short capillary force-driven stage, after which the particle settles at the interface, and the subsequent dissolution, locally enhanced by Marangoni flow affecting the particle morphology, after which the particle finally detaches and dissolves completely in the slag phase.

The modelling of these effects was compared to experimental in-situ observations of particle dissolution at a slag-argon interface, carried out in a high-temperature confocal laser-scanning microscope (HT-CLSM) setup, where the phenomenon could be confirmed visually. Figure 2 shows the detachment of a soluble particle at the slag-argon interface as observed in the HT-CLSM setup [8], where both process stages of initial settling at the surface and the subsequent immersion/ dissolution process until final detachment from the interface can be clearly identified. The challenges were to achieve a realistic depiction of an inclusion at a two-fluid interface in lab-scale crucibles, and to find transparent slag material to allow for the visual inspection of the process. Increased dissolution has been observed close to the interface, where Marangoni convection plays a role in locally enhancing the dissolution rate, also leading to a morphology change in the inclusion particle (pear shape) before final detachment.

In summary, important effects for particle dynamics like capillary forces, viscosity effects and Marangoni convection around particles have been modelled, and the effect of material parameters like the fluid viscosity, the wetting angle and inclusion material properties have been explored. Ultimately, quantitative criteria of these phenomena have been derived, which were then further used in the modelling of large-scale processes.

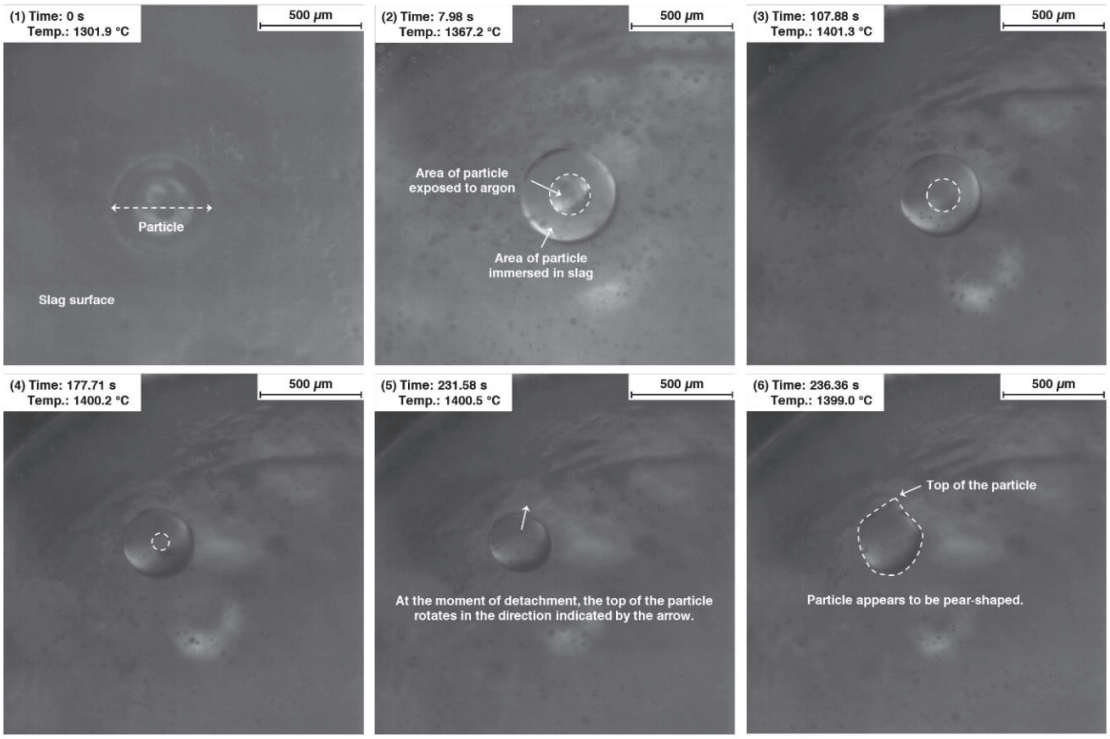

FIGURE 2. A $MgAl_2O_4$ spinel particle detaching from the slag surface observed during the HT-CLSM experiment. [8]

NMI removal in the tundish

The detailed model of NMI separation in a multiphase fluid flow has been implemented into the larger geometry of a generic tundish and considered in the cases with and without gas injection in the tundish [9].

A test block and a generic tundish geometry, respectively, have been set up as ANSYS Fluent simulation cases, in which the detailed dynamics of inclusion particle separation has been implemented. The simulation case again implements a VOF formulation for the liquid steel and slag, while inclusion particles as well as argon injection are both represented by Lagrangian particles using the discrete phase model (DPM). For the injected gas a volume fraction field of the gas phase is computed for modelling the interaction of the gas phase with NMI particles.

The simulation model was set up with PISO pressure-velocity coupling using the QUICK discretization scheme for the momentum equation and PRESTO for the pressure interpolation. Turbulence was modelled using the k-omega SST turbulence model. Computation times are different for the flow field and NMI movement, respectively, and also different process time spans have been investigated. The calculation was done on a small local cluster only.

In a first step, the fluid flow is computed to yield a stationary flow field. Subsequently, the trajectories of inclusions and argon bubbles are computed on a frozen flow field. When inclusion particles and argon bubbles intercept, the probability for inclusions to be attached to the gas phase is calculated based on a criterion developed in [10], and the trajectory of the inclusion is henceforth assumed to be the trajectory of the bubble. The criterion gives an attachment probability for an inclusion to a bubble in dependence of bubble and inclusion sizes, obtained by regression of numerical parameter studies, as

$$P = C_A d_P^{C_B},$$

where C_A and C_B are fitted polynomials of bubble diameter d_B and inclusion diameter d_P, measured in mm and µm, respectively [10]. A later detachment of the inclusion from the bubble is not considered. This is based on the assumption that bubbles are significantly larger (diameters between 1 and 10 mm, as are common in continuous casting) than NMIs (sizes in the range of µm), and that the momentum of NMIs in comparison to bubbles can be neglected, i.e., the collision of NMIs with bubbles do not affect bubbles' trajectories. In cases without gas injection in the tundish, this effect does not contribute to the NMI removal. As soon as those inclusions are captured by a gas bubble, they are removed from the simulation. When inclusions do not meet gas bubbles, but directly reach the steel-slag interface through the natural buoyancy and flow dynamics, they are separated into the slag phase based on the

separation criterion developed in [4] [5] [8], and then deleted from the simulation. The model does not take into account any further evolution of inclusions after their absorption and dissolution into the slag phase. For simplicity, phenomena like slag entrainment or other effects leading to a return of inclusions into the steel phase have not been explicitly modelled.

Figure 3 shows the implementation of the inclusion removal mechanism into (a) a generic test block, and (b) a generic large-scale tundish geometry, done with the ANSYS Fluent CFD package. These investigations serve to explore the NMI removal efficiency in the tundish phase of continuous casting and help to explore and understand different operational modes like gas injection, different casting speeds or steel grades.

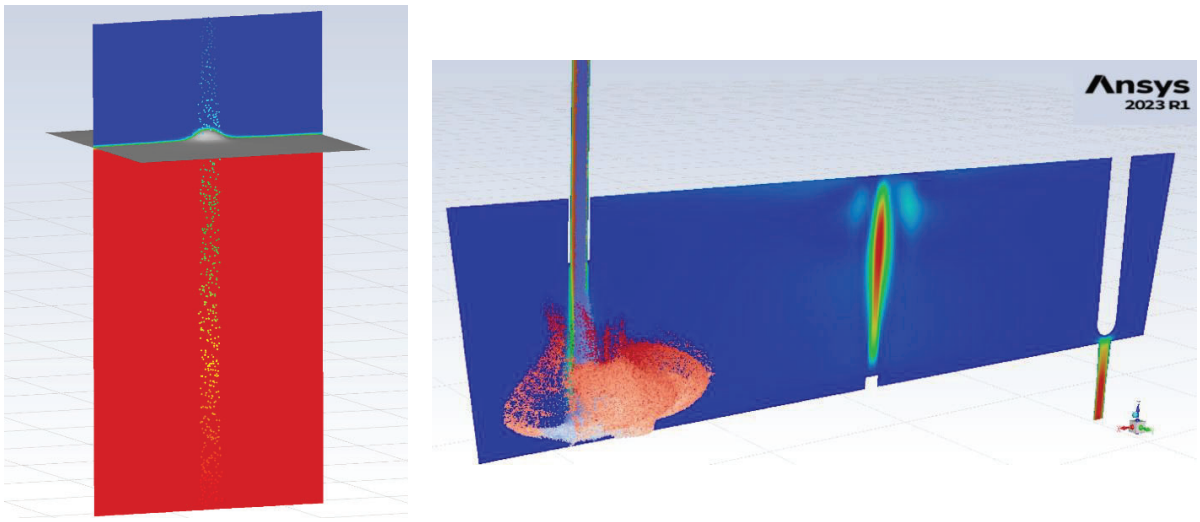

(a) (b)

FIGURE 3. NMI separation [9]. Fluid flow in (a) test block with inclusion removal mechanism, (b) academic tundish geometry with inclusion removal mechanism. The color scheme in (a) shows the liquid phases (red for steel and blue for slag), the steel-slag interface in grey and the ID of the injected particles. The colors in (b) represent the liquid phase velocity as well as the ID of the injected particles.

Modelling different clogging mechanisms in multiphase fluid flows

The importance of NMIs for the clogging phenomenon in continuous casting of steel is well known and has been subject of many investigations by simulations and experiments. A review of experimental activities can e.g., be found here [11]. On the simulation side, extensive activities have focused on the description of NMI behavior in the SEN, where clogging is the determining factor for regular process operation and lifetime of plant components.

In a series of papers, Barati et al. have defined a comprehensive framework to describe the clogging phenomenon, from a basic transient model with a Euler phase for the turbulent flow, and Lagrangian phase for solid inclusion particles (see [12] for the base model and [13] [14] [15] [16] [17] for subsequent improvements and adaptations of the model). In the clogging process, different steps have been identified: (a) chemical reactions between steel and refractory lead to the formation of a first oxide layer at the SEN walls, called early stage of clogging, (b) turbulent fluid flow transports the particles towards the SEN walls, (c) attachment of the particles on the wall modelled by a dynamical change in wall roughness (clog still stays within the boundary computational cell), (d) growth of the clog leading to the build-up of a layer of porous medium (stabilized by high temperature sintering), called late stage of clogging, and resulting in a modification of the fluid flow; hence, two-way coupling between the melt flow and the clog growth has to be taken into account, (e) destruction of the clog structures by the forces exerted by the fluid flow around and through them, leading to the fragmentation of the clog. The major steps of clogging are depicted in Fig. 4.

Euler-Lagrange simulations [12] for these phenomena have been set up with specific sub-models for the clog growth and fragmentation. Due to the very small size of the particle comparing to the typical computational cell size, a volume-average approach has been adopted to taken formation and change of clog into account. Generally, three phases can exist in a computational cell: liquid steel, dispersed solid particles, and porous solid clog. For liquid steel, an isothermal incompressible one-fluid model with constant material properties throughout the bulk has been assumed. Turbulence has been modelled with both scale adaptive simulation (SAS) and shear-stress transport (SST) k-ω models,

and force terms for buoyancy, drag, lift, virtual mass and pressure gradients have been included for the Lagrangian tracking of particles. In the computation of the model, the usual equations for mass, momentum, turbulence kinetic energy and specific dissipation rate are solved (more details can be found in [12]- [17]). The commercial CFD code ANSYS Fluent (finite volume method) was used to solve equations with extended user-defined functions (UDFs) for considering tracking, attachment, and detachment of solid particles as well as the growth of the clog. Computations are done on a high-performance computer cluster with 30–48 CPUs (2.6 GHz). A simulation of a one-hour period of the process took approximately 12 days.

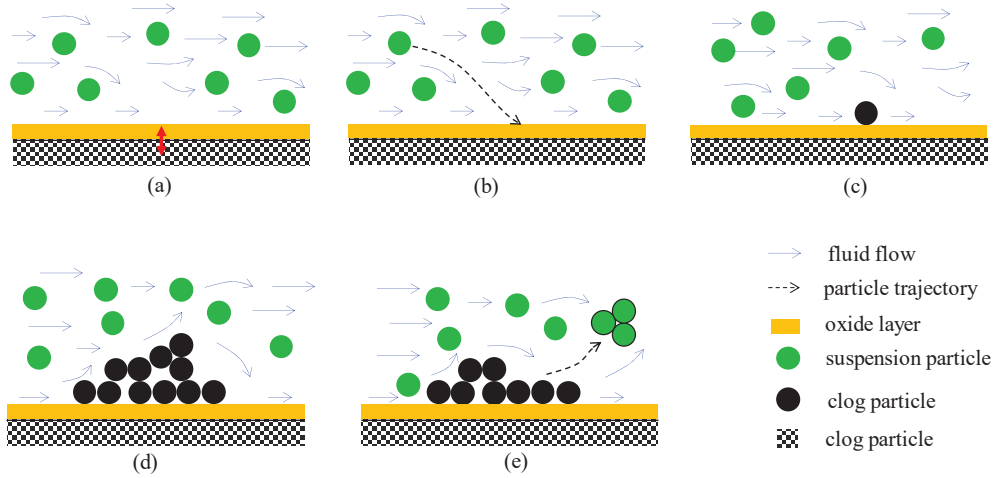

FIGURE 4. Schematic of main steps of clogging [16]. (a) formation of the first oxide layer by chemical reactions; (b) transport of NMIs; (c) adhesion of the NMI on the SEN wall; (d) growth of the clog; and (e) detachment/ fragmentation.

The multi-stage clogging model has been validated by comparison [12] with experimental data from the literature [18] [19], as well as by investigations of industrially used SENs [17] [20]. An exemplary evolution of clogging over time can be seen in Fig. 5, where (a) shows the stages of increasing clogging in the SEN halves, and (b) shows the corresponding local clog thickness at a certain point in the middle of the tube part of the SEN (blue line) and the derivative of this thickness with regard to time, i.e. clog rate (red line). The local clog thickness shows an almost continuous growth of the clog, but the slope of this curve is not always positive. This is due to the fact that sometimes in some time steps, the volume of the deposited particles is smaller than the volume of the detached particle in a computational cell at the clog interface. Therefore, the clog rate can become minimally negative in such instances. High- and low-frequency oscillations are due to changes in local flow behavior during the time that leads to higher or lower attachment/ detachment ratio at the clog interface.

The models' calculation accuracy and efficiency have been evaluated in dedicated CFD studies, investigating the dependence of simulation results on the choice of meshing as well as the "number of representative particles" introduced to handle large numbers of real particles [13].

Solidification has been implemented with an enthalpy-based mixture continuum model [14], which adds an enthalpy equation as well as additional source terms to mimic the mushy zone where the transition between fluid and solid phase takes place. The aim of these investigations was to explain the presence of solidified (i.e., frozen) steel in samples of industrially used SENs. The study concluded that the solidification of steel in SENs occurs only after certain level of clogging has taken place, and in so-called open-channel clog regions, some sort of porous clog structures, where clog fragmentation does not occur anymore. If the steel is sufficiently superheated and also the SEN is preheated, then clogging is not strong enough to allow for solidification of steel.

The early stage of clogging, i.e., the formation of a first oxide layer by chemical reactions between steel and refractory in the SEN, has been investigated in more detail in a mathematical model [15] for the example of a Ti-treated ultra-low-carbon steel, where reactions of alumina, titanium and iron in the steel with the CO gas produced by reactions of graphite and silica in the refractory at elevated temperatures take place. Currently this model extension is only available for Ti-ULC steel grade which is very sensitive to clogging [17]. Although the contribution of early-stage in total clogging thickness is very small, around 2 – 3% [17], it provides the initial substrate for further deposition of solid particles which is the major part. In other words, the early-stage promotes the later-stage of clogging.

Fragmentation [16] [17] is an important phenomenon, which counterbalances the build-up of clog material, slowing down the clogging process. The importance of fragmentation was recognized by contrasting the results of the clogging models with experiences from the industrial casting process. Without fragmentation, clogging models would predict much stronger clogging, which is however not observed in industrial situations. It is thus necessary to include the fragmentation model into the clogging simulation framework. To account for fragmentation, NMIs are assumed to form forests of clog fingers, consisting of NMIs bound together by a sintering effect due to high temperatures. Then, the stress due to the hydraulic drag force in the fluid is calculated and exerted on the assumed clog fingers, determining the effective clog growth.

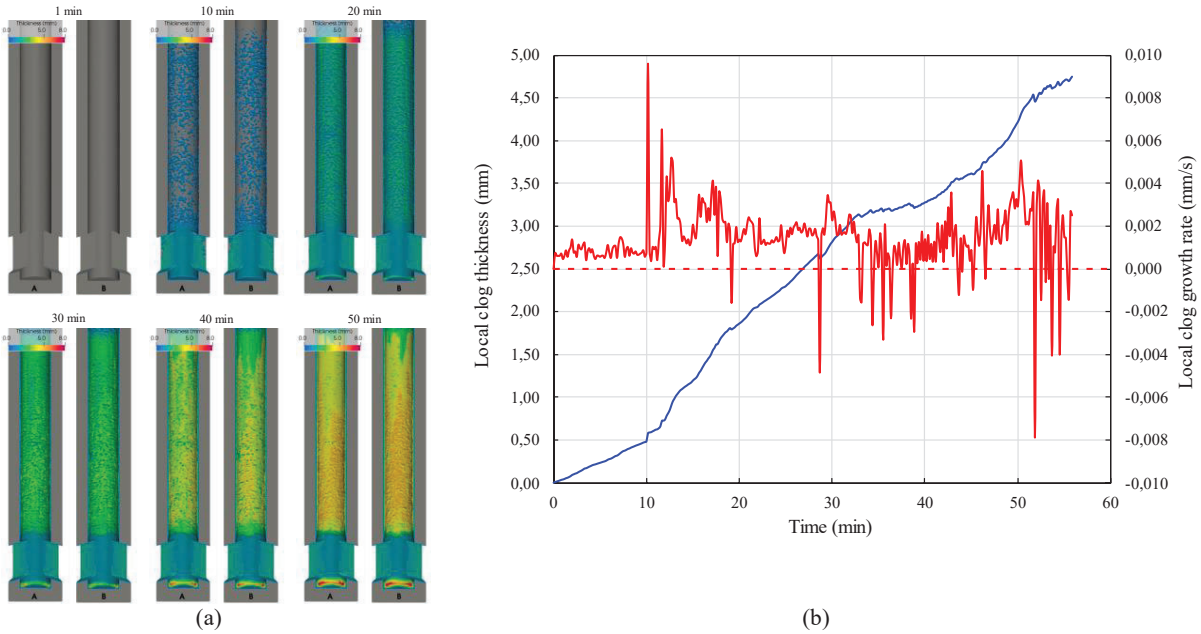

(a) (b)

FIGURE 5. (a) Evolution of clogging in the SEN (two halves on left and right, after 1, 10, 20, 30,40, 50 min), color scheme indicates clog thickness between 0 and 8 mm (color bar at the top left of each clogging stage), (b) Evolution of local clog thickness and clog growth rate. Both from [17].

The model represents a comprehensive framework of different relevant phenomena and process stages. However, there are some aspects that have not been taken into account yet. For instance, the fluid model does not include a gaseous phase, which is usually present due to the argon injection in the SEN in industrial applications. The presence of gas bubbles is expected to alter the flow behavior and the pressure distribution in the SEN [21], and may lead to a different clogging evolution in the SEN. It is believed that gas bubbles hinder clogging in the SEN by capturing solid inclusions and carrying them through the SEN into the mold. In the mold region, bubbles float up and reach the mold slag, therefore providing an additional possibility to remove inclusions. A changed pressure distribution due to gas injection will also affect the chemical reactions between steel, refractory, and inclusions. Phenomena like cavitation in the SEN or effects caused by temperature variations or compressibility are also not yet modelled.

With respect to validation, further activities are planned in the comparison of the clogging model to used SENs from industrial operation, in particular with respect to different compositions of the materials involved. Comparisons have been done only for a few select cases (see e.g., Fig. 13 in [12], where a general qualitative agreement has been found), and thus further validation needs to be extended to different steel grades and clogging stages.

Modelling mold flows

Continuous slab casting mold flows have been modelled in transient numerical simulations using the ANSYS Fluent CFD package considering a liquid phase, movement of gas bubbles and solid particles in typical geometries of continuous casting molds. The injection of argon gas at the top of the SEN is a common measure to reduce the clogging effects. The gas forms bubbles that are transported by the melt flow into the mold. Due to their buoyancy, the bubbles rise to the mold top surface and influence the mold flow pattern. The argon injection rate has to be carefully adapted to the casting parameters in order to achieve an advantageous flow pattern for a good product quality. In those

investigations of bubbly mold flow in continuous casting [22], different numerical models have been proposed and compared.

In a first step, only single-phase flow has been considered, and the realizable k-ε (RKE) and SAS turbulence models have both been applied for the example of a water-air flow scenario. The SAS model is capable of better resolution of turbulent features, but this results in an increased cost of computation due to a 10 times smaller time step necessary (RKE: 0.01 s, SAS: 0.001 s). For both models, the same computational grid is used, consisting of 774 000 hexahedral cells. Second order upwind discretization schemes are used for all equations except or the SAS model, where a bounded central difference scheme is used for the momentum equation. To obtain time averaged results from the transient simulations, 120 s of process time were calculated. Such a computation with the SAS model needs 36 hours on 32 AMD EPYC cores. Both models have been contrasted with experimental investigations of the flow pattern recorded in a 1:1 scale water model of a continuous caster at voestalpine Stahl Linz GmbH. This experimental facility features tundish, SEN and mold built in acrylic glass, where the flow pattern and bubble distribution can be monitored by camera equipment and evaluated with particle image velocimetry (PIV) techniques. PIV measurements are available from both surfaces parallel to the wide and narrow faces of the mold. At the mold top surface, the bubbles at the surface carried by the surface water flow are used as tracer objects to determine the flow velocity field with the PIV algorithm even for high gas loads, where the bubbles render the interior of the mold intransparent and therefore prevent PIV measurements on interior surfaces. However, the deduction of flow velocities in this case could be invalid if the bubbles do not move with the same velocity as the carrying water phase. Considering the different properties of the systems steel-argon and water-air, qualitative coincidence of flow parameters like casting speed and gas injection rates can be achieved by imposing Reynolds and Froude similarity of the flows.

Flow patterns and the distribution of the turbulent kinetic energy are compared qualitatively between results from the RKE model, the SAS model, and the experimental PIV measurements, respectively. In this comparison it has been shown that important characteristics of turbulence in mold flows, such as the direction and shape of the SEN jet at the port and the meniscus surface flow patterns cannot be reproduced well in the RKE model but require the more exact SAS model. Grid independence of either simulation method could however not be proven in this study, and no grid independence checks for the SAS model could be found in the literature. Moreover, the effect of displacement of liquid by bubbles has been neglected in these investigations.

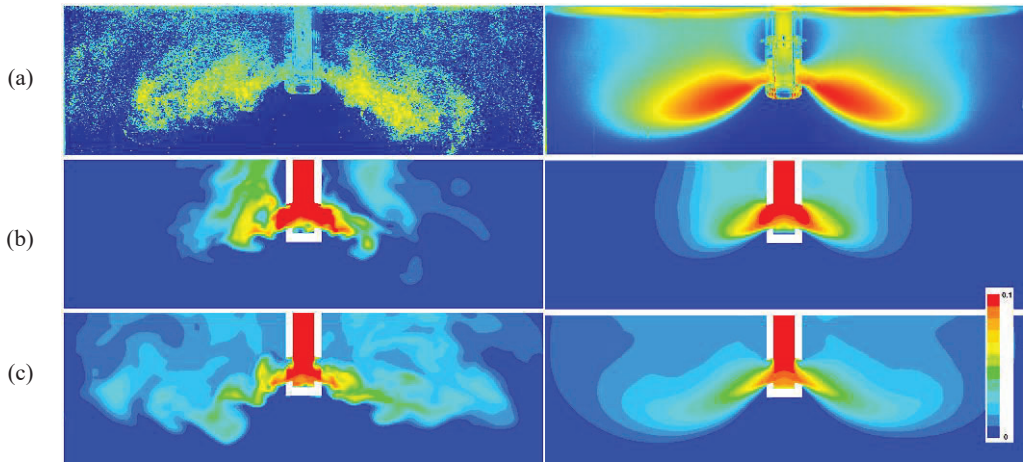

FIGURE 6. Comparison of mold flows via the qualitative illustration of the gas volume fraction in the mold center plane [23] (left column: snapshots, right column: average over 120 s). (a) Experimental evaluation of camera image brightness, qualitatively correlating with the gas volume fraction, (b) SAS model with conventional drag law, (c) SAS model with modified Brucato drag law for bubble motion (both (b) and (c) contour colors show the dimensionless volume fraction according to the color bar in the corner).

In a next step, gas injection through the SEN into the mold has been modelled with a Eulerian model for the gas volume fraction field. Bubbles are not resolved individually but modelled as a secondary phase by solving a transport equation for the bubble volume fraction. The impact of turbulence on the bubble motion has been captured by implementing a modified drag law proposed in [24] taking into account a reduced bubble drift velocity due to turbulent flow patterns. This drag law modification leads to a slower rise of bubbles in regions of higher turbulence, i.e., inside of the jets the SEN. Results with and without the modified drag law were again contrasted with experimental observations of mold flows in the water model. Exemplarily, a comparison of the gas volume fraction in the mold

center plane is shown in Fig. 6, comparing (a) the experimental evaluation, (b) the SAS model with the modified Brucato drag law, and (c) the SAS model with conventional drag law. It is clear that (b) is in much better correspondence to the experimental results than (c), and thus the drag modification due to turbulence is essential for the correct transport of gas bubbles by nozzle jets. Further variations of the modelling approaches can be found in [22], in particular also for the RKE model and variations for different gas injection rates. Also the flow pattern behavior at the mold top surface has been investigated, and in particular for higher gas injection rates, the transition from a double roll to a single roll pattern as observed in experiments, can only be reproduced by the SAS model, but not by the RKE model. Again, the SAS model is thus confirmed as a realistic model for mold flows, whereas the RKE model should be discarded as not appropriate.

The 1:1 scaled water model has been the subject of further investigations of turbulent flows in [23]. In addition to the visual inspection of the flow situation, also direct measurements of the mold surface flow velocities with immersed paddles were performed. A comparison of the mold surface velocities obtained with both PIV and paddle measurements resulted in some discrepancies. These are possibly due to the interference of paddles with the flow and PIV measurements, due to the position of the paddle head, which is slightly submerged into the mold in contrast to the PIV measurement of bubble movement on the surface, or due to a mismatch in bubble and flow velocities. Moreover, bubble diameters were qualitatively assessed, resulting in a rather uniform bubble size distribution around 5-6 mm. For this size range of bubbles, the rising velocity is nearly constant, i.e., independent of the exact bubble size. Very few bubble breakup or coalescence effects have been detected.

The agreement of these experimental investigations with simulation results have shown to be very good, and requirements for realistic simulation models have been determined. Further investigations can be done towards refining the experimental evaluation methods with PIV or paddle techniques, and validation will be extended towards a broader range of process parameters. Ultimately, a transfer of simulations to a scenario involving steel and argon will be done, and validation with industrial data and experiences will be attempted. First simulations of the casting process with NMIs for both without and with gas show that the gas reduces the NMI concentration peaks in the slabs as it homogenizes the flow in the strand [25].

Steel flows through a clogged SEN

From the numerical simulations of SEN clogging, also the modified fluid flow patterns through a clogged SEN can be extracted. Using the setup for clogging simulations described above, a visualization of SEN flows in Fig. 7 shows the flow irregularities in the SEN port for three different levels of clogging.

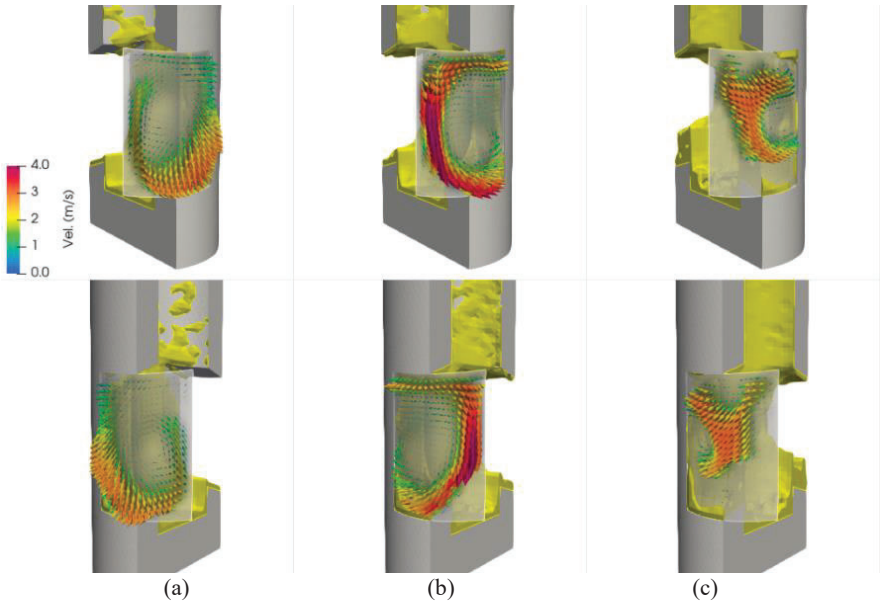

FIGURE 7. Flows at the SEN port for right (upper row) and left (lower row) port, for different levels of clogging (a, b, and c).

The clogging effect leads to a modified fluid flow at the SEN port and thus is expected also to affect the mold flow pattern to deviate from the ideal conditions The numerical simulation of mold flows as described in [22] has been further generalized to considering a clogged SEN, using the clogging simulations as described above as a boundary

condition for the simulation of the SEN and mold flows to assess the impact of the clogged SEN on the mold flow. To model the clogged regions as porous medium in a combined SEN and mold simulation, the simulation was set up according to [22] with an SAS turbulence model, Eulerian phase modelling of gas bubbles and the modified Brucato drag model. To account for clogging, corresponding particle volume fractions were provided from the clogging simulation for clogged regions. The modelling of the porous medium in the clogged SEN was moreover simplified and substituted for better numerical handling by an empirical model,

$$f_i = -c\, f_P\, u_i\,, \tag{3}$$

where f_i are the source terms in the momentum equation to account for the flow braking forces caused by clog material (dimension force per volume), f_P is the volume fraction of particles (dimensionless), u_i are the components of the velocity field vector, and c is an empirically determined constant with $c = 10^7\ \frac{N/m^3}{m/s}$. The value was chosen as high as possible without running into solver divergence problems.

Results for the simulation of flow patterns at the mold top surface are shown in Fig. 8, where the flow field at the meniscus is depicted, and an average over 180 seconds for different simulations has been computed. In general, flow patterns can be compared only qualitatively since flow amplitudes are scaled differently. Still, it could be confirmed that clogging leads to asymmetries in the top surface flow across the symmetry line in mold width direction, as compared to the scenario without SEN clogging. Where the simulation with the non-clogged SEN in Fig. 8(a) shows an even symmetric flow distribution towards the SEN, the different simulations for clogged SENs at different clogging levels (b-d) show deviations of the flow towards the wide faces of the mold as well as asymmetries between the two halves of the mold. This depicts very well the problematic consequences of clogging on the subsequent stages of casting.

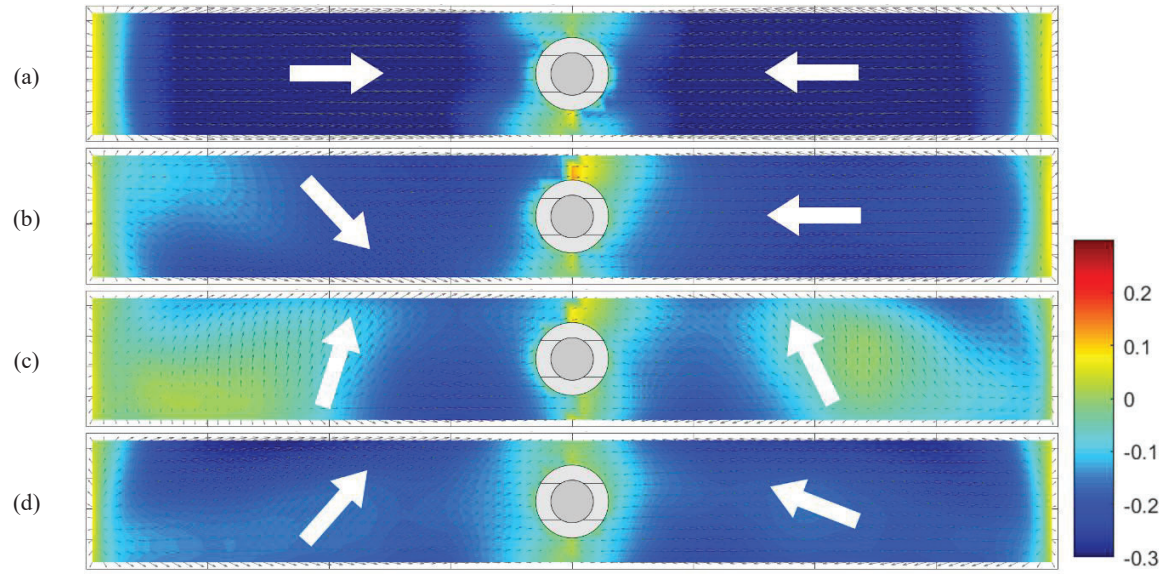

FIGURE 8. Time-averaged mold flow field at the meniscus for different states of clogging illustrated by velocity vectors and contours of the velocity component parallel to the mold wide face in direction of the mold center, color scale in m/s. (a) without clogging, (b) light clogging, (c) moderate clogging, (d) strong clogging. The flow pattern for the non-clogged SEN (a) is clearly different to the ones for the clogged SENs (b-d), and asymmetries in the meniscus flow are clearly visible.

SUMMARY OF NUMERICAL MODELS AND RESULTS

In summary, the paper has shown different detailed models for multiphase fluid flows as they occur in the industrial continuous casting process. The different model approaches introduced in this paper have been developed separately but have then been combined to result in process models depicting realistic conditions as in the continuous casting process. In the case of NMI separation in the tundish, a microscopic model for the separation of NMIs into the slag phase has been developed numerically and validated with experimental investigations. Subsequently, the microscopic model has been implemented into a macro-scale model of a tundish flow, which can be used to evaluate and monitor the NMI separation process on larger scales and for different process conditions. Small-scale investigations on particle

behavior at the steel-slag interface therefore contribute to an increased understanding of interfacial phenomena in the process of inclusion removal relevant in large-scale metallurgical vessels.

Clogging of SENs has been modelled by investigating microscopic phenomena like early-stage clog layer formation, attachment of NMIs to the SEN walls, and growth and fragmentation of clog structures. From these investigations, insights into the clogging behavior can be obtained to optimize SEN usage in continuous casting on a macro-scale. Moreover, the simulation of mold flows serves to an increased understanding of the multiphase flow behavior in the mold, and different configurations of SEN clogging can be investigated to evaluate the impact of clogging on the mold flows and subsequent solidification behavior of steel.

OUTLOOK

Apart from the improvements planned on the theoretical side to address the aforementioned shortcomings of the introduced models, several activities towards further development of the modelling of continuous casting are ongoing.

The behavior of NMIs in the tundish can be further extended to account for the NMI interactions with bubbles and could also be applied to other similar tundish geometries or qualitatively different setups like bloom casters.

Further investigations are also in progress on the validation of the clogging model with plant data, in particular, with temperature and pressure measurements along the SEN, as well as by investigating the geometry of industrially used clogged SENs to compare with clogging predictions from the models.

Industrial casting data will be used in a first step, and in the future, also more extensive experimental measurements will be done in plants and experimental lab facilities. In its current setup, the clogging model requires significant time spans and computational power to achieve the simulation of industrially relevant time scales. Another goal is thus to extract the relevant dynamics from the model in a simplified form, allowing the application towards industrial settings for various operational conditions. This makes the simulations feasible as a prediction model of clogging that can be employed in-line with the production process.

As mentioned in [22], the numerical simulations of mold flows have so far only been validated with experiments for certain flow conditions and using a model with a mixture of water and air. As a next step, validation activities will be extended towards a broader range of process parameters, considering more variations of gas injection rates, casting speeds, SEN immersion depth and mold dimensions.

The implementation of the geometry of industrially clogged SENs into mold flow simulations will be attempted, to better understand the impact of real industrial clogging on the flow situation.

Furthermore, the conditions in liquid metal will be explored both in numerical activities, where simulations for realistic industrial process conditions using steel and argon injection will be done, and in an experimental setup using a low-melting BiSn alloy casting simulator setup currently in development [26] [27].

ACKNOWLEDGMENTS

The authors gratefully acknowledge the funding support of K1-MET GmbH, metallurgical competence center.

The research program of the K1-MET competence center is supported by COMET (Competence Center for Excellent Technologies), the Austrian program for competence centers. COMET is funded by the Federal Ministry for Climate Action, Environment, Energy, Mobility, Innovation and Technology, the Federal Ministry for Digital and Economic Affairs, the Federal States of Upper Austria, Tyrol, and Styria, as well as the Styrian Business Promotion Agency (SFG). In addition to the public funding from COMET, this research project was partially financed by scientific partners (Montanuniversität Leoben and Johannes Kepler University Linz) and industrial partners (voestalpine Stahl Linz GmbH, voestalpine Stahl Donawitz GmbH, and RHI Magnesita GmbH).

REFERENCES

1. Y. Miki und B. Thomas, “Modeling of inclusion removal in a tundish,” Metallurgical and Materials Transactions B **30**, 639–654 (1999).
2. K. Raghavendra, S. Sarkar, S. Ajmani, M. Denys und M. Singh, “Mathematical modelling of single and multi-strand tundish for inclusion analysis,” Applied Mathematical Modelling **37**, 6284-6300 (2013).
3. Y. Nakajima, “Effects of both flux compositions and oxidizing conditions on the dephosphorization of high-chromium hot metal,“ in *4th International Conference on Molten Slags and Fluxes*, Sendai, Japan, 1992.

4. X. Zhang, S. Pirker und M. Saeedipour, “Numerical investigation of particle motion at the steel—slag interface in continuous casting using VOF method and dynamic overset grids,“ Experimental and Computational Multiphase Flow **5**, 178–191 (2023).
5. X. Zhang, S. Pirker und M. Saeedipour, “Investigation of Inclusion Removal at Steel–Slag Interface toward a Small-Scale Criterion for Particle Separation,” Steel Research International **94**, 2200842 (2023).
6. C. W. Hirt und B. D. Nichols, “Volume of fluid (VOF) method for the dynamics of free boundaries,” Journal of Computational Physics **39**, 201–225 (1981).
7. J. Brackbill, D. Kothe und C. Zemach, “A Continuum Method for Modeling Surface Tension,” Journal of Computational Physics **100**, 335-354 (1992).
8. X. Zhang, S. Michelic, S. Pirker und M. Saeedipour, “Detachment of a Soluble Particle at the Slag-Argon Interface: CFD Study and Experimental Observations,” Metallurgical and Materials Transactions B **55**, 1442-1454 (2024).
9. G. Holzinger, X. Zhang und e. al., “TBD,“ in *Liquid Metal Processing Conference*, Leoben, Austria, 2024.
10. L. Zhang, J. Aoki und B. Thomas, “Inclusion Removal by Bubble Flotation in a Continuous Casting Mold,” Metallurgical and Materials Transactions B **37**, 361-379 (2006).
11. S. Michelic und C. Bernhard, “Significance of Nonmetallic Inclusions for the Clogging Phenomenon in Continuous Casting of Steel - A Review,” Steel Research International **93**, 2200086 (2022).
12. H. Barati, M. Wu, A. Kharicha und A. Ludwig, “A transient model for nozzle clogging,“ Powder Technology **329**, 181-198 (2018).
13. H. Barati, M. Wu, A. Kharicha und A. Ludwig, “Calculation Accuracy and Efficiency of a Transient Model for Submerged Entry Nozzle Clogging,” Metallurgical and Materials Transactions B **50**, 1428–1443 (2019).
14. H. Barati, M. Wu, A. Kharicha und A. Ludwig, „Role of Solidification in Submerged Entry Nozzle Clogging During Continuous Casting of Steel,“ Steel Research International **91**, 2000230 (2020).
15. H. Barati, M. Wu, S. Michelic, S. Ilie, A. Kharicha, A. Ludwig und Y.-B. Kang, “Mathematical Modeling of the Early Stage of Clogging of the SEN During Continuous Casting of Ti-ULC Steel,” Metallurgical and Materials Transactions B **52**, 4167–4178 (2021).
16. H. Barati, M. Wu, A. Kharicha und A. Ludwig, “Transient simulation of melt flow, clogging, and clog fragmentation inside SEN during steel continuous casting,“ IOP Conference Series: Materials Science and Engineering **1281**, 012025 (2023).
17. H. Barati, M. Wu, S. Ilie, A. Kharicha und A. Ludwig, “Numerical modeling of clog fragmentation during SEN clogging in steel continuous casting,“ Powder Technology **434**, 119307 (2024).
18. D. Janis, A. Karasev, R. Inoue und P. Jönsson, “A Study of Cluster Characteristics in Liquid Stainless Steel and in a Clogged Nozzle,” Steel Research International **86**, 1271-1278 (2015).
19. Z. Deng, M. Zhu, Y. Zhou und D. Sichen, “Attachment of Alumina on the Wall of Submerged Entry Nozzle During Continuous Casting of Al-Killed Steel,” Metallurgical and Materials Transactions B **47**, 2015–2025, (2016).
20. U. Diéguez Salgado, P. Dorrer, S. Michelic und C. Bernhard, “Experimental Investigation of the System Nonmetallic Inclusion-Molten Steel-Refractory System at High Temperatures,” Journal of Materials Engineering and Performance **27**, 4983–4988 (2018).
21. S. Pirker, D. Kahrimanovic und S. Schneiderbauer, “Secondary Vortex Formation in Bifurcated Submerged Entry Nozzles: Numerical Simulation of Gas Bubble Entrapment,” Metallurgical and Materials Transactions B **46**, 953-960 (2015).
22. M. Javurek und R. Wincor, “Bubbly Mold Flow in Continuous Casting: Comparison of Numerical Flow Simulations with Water Model Measurements,” Steel Research International **91**, 2000415 (2020).
23. F. Brucato und G. M. Grisafi, “Particle drag coefficients in turbulent fluids,” Chemical Engineering Science **53**, 3295-3314 (1998).
24. M. Javurek, M. Brummayer und R. Wincor, “Turbulent flow measurements in continuous steel casting mold water model,” Materials Today: Proceedings **62**, 2581-2586 (2022).
25. M. Javurek und S. Ilie, “Simulation of flow-induced inclusion deposition in a continuous casting strand,” in *6th European Steel Technology and Application Days (ESTAD)*, Düsseldorf, Germany, 2023.
26. P. Ramirez Lopez, J. Bjorkvall, C. Olofsson, P. Nazem Jalali, U. Sjostrom und C. Nilsson, “Continuous Casting Simulator for Measurement and Control of Liquid Metal Flow in the Mould,” in *8th European Continuous Casting Conference*, Graz, Austria, 2014.